

Real-Time Control of Plasma Instabilities

Numerical investigations of real-time control of tearing modes with current drive

Inês Sousa Borges de Almeida¹

Under Supervision of Prof. Paulo Oliveira² and Prof. Nuno Loureiro¹

¹*Instituto de Plasmas e Fusão Nuclear, Instituto Superior Técnico, Lisboa, Portugal*

²*Departamento de Engenharia Mecânica, Instituto Superior Técnico, Lisboa, Portugal*

(Dated: September 2013)

Tearing modes are a type of instability that occurs in fusion devices, and are one of the main obstacles to having a long lasting, sustainable reaction. In this work, the problem of tearing mode control by current injection is studied. The study is made through the numerical simulation of a tearing mode in slab geometry. Several spatial profiles and amplitudes for the injected current are tested. It is concluded that it is possible to control the instability by driving current either into the X-point or into the O-point of the island. The current's amplitude is determined by two different approaches, one based on the theoretical knowledge of this instability, and another one based on linear control theory. In both cases, the current's amplitude depends only on variables that would be available in a real fusion experiment. These quantities are determined using methods that simulate real-life diagnostics. Both approaches produce good results and are shown to be worthy of further investigations.

Keywords: magnetic confinement fusion; plasmas; instabilities; real time control; tearing modes; current drive.

I. INTRODUCTION

Tearing modes and neoclassical tearing modes (NTMs) are one of the most important kinds of instabilities that can occur in a magnetic confinement fusion plasma [1]. These instabilities are responsible for confinement degradation and plasma disruptions [2]. The control of tearing modes is a topic of major importance, and the main focus of this work.

Although classical tearing modes and neoclassical tearing modes are similar, they have different triggering mechanisms. They both manifest themselves through the appearance of “magnetic islands”, see Fig. 1. Classical tearing modes, or simply tearing modes [3, 4], arise from finite resistive effects which are dominant at the so-called rational surfaces, where the safety factor [1, Sec. 3.4] q is rational, that is, equal to m/n with m, n integer numbers. Here, m and n are the poloidal and toroidal mode numbers, respectively. Around this surface, ideal magnetohydrodynamics fails and a more complete model, namely one which includes resistivity, viscosity and other non-ideal effects, is required. Neoclassical tearing modes [5, 6] result from a perturbation of the bootstrap current [1, Sec. 3.10]. If there is a local flattening of the pressure profile due to the presence of a seed magnetic island, the bootstrap current is locally reduced. The lack of bootstrap current causes the magnetic island to grow, which in turn flattens the pressure profile even more. This mechanism makes the island grow until a saturation width is reached. Unlike classical tearing modes, NTMs require the existence of a seed island which must be large enough to perturb the pressure profile [7].

Tearing modes are often associated with magnetic islands, periodic structures which are formed after the breaking and reconnection of the magnetic

field lines. Inside these magnetic islands the pressure and temperature profiles are flattened because the island works as a short-circuit which allows particles and heat to flow radially across the island [8]. The consequences of these effects on plasma confinement, namely on the confinement time τ_E , were studied in [8]. A degradation of up to 50% of the confinement time when a $m/n = 2/1$ mode occurs was predicted. Tearing modes can also lock to the wall of the vessel, a process which slows the plasma rotation until it eventually stops rotating, which compromises the confinement [9].

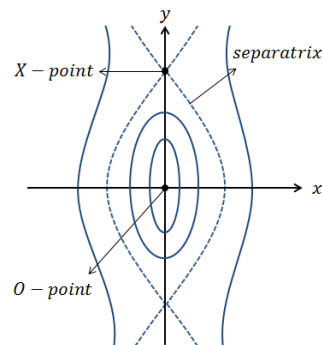


Figure 1: Schematic representation of a magnetic island. The dashed line is the separatrix of the island.

There are several approaches to NTM control. These are divided among preventive strategies, which are based on avoiding the triggering of tearing modes, and active control strategies, which attempt to suppress a tearing mode whose appearance could not be avoided. Preventive measures include sawtooth control [10, 11], profile control [12] and plasma shaping. Active control can be achieved via entering the frequently interrupted regime (FIR) [13, 14] or injecting current using electron cyclotron resonance heating (ECRH), current drive (ECCD) [15, 16], or lower hybrid current drive

(LHCD) [17].

There are many excellent reviews on the topic of tearing mode and NTM control. Chapter 3 of the Nuclear Fusion special issue, Progress in the ITER Physics Basis, is a comprehensive, compilation covering (in)stability, including sawteeth and NTM physics and control strategies, and disruption [2]. La Haye [6] wrote a complete review on NTM control, describing both the theory and the control of these instabilities. The sections dedicated to the International Thermonuclear Experimental Reactor (ITER) in these documents are slightly outdated, and a more recent review by Maraschek [18] includes newer results and an analysis of their consequences for ITER. Electron Cyclotron Current Drive (ECCD) [19] has become the method of choice for tearing mode stabilization due to its localized deposition [20], and the control of tearing modes by current injection is the main focus of this work.

This work focuses on studying the control of tearing modes by current drive. The study is performed by means of numerical experiments. Several profiles for the driven current, namely Gaussian profiles centered around the X- and O-points of the island, are compared. The influence of the amplitude of the injected current on the evolution of the island is also studied. Two distinct approaches are followed in order to determine what the amplitude of the driven current should be. One of them relies on analytical estimates based on the theory of non-linear tearing mode evolution, and the other one is based on optimal linear control theory. In both cases, the amplitude of the current depends only on quantities that are measurable in a real-life experiment. These quantities are determined using methods that simulate real-life diagnostics.

The remainder of this document is organized as follows: Section II briefly describes the model which was adopted to perform the numerical experiments. The natural evolution of the system, *i.e.*, when no control is attempted, is described in Section III. The two approaches used for controlling the island, together with the main results that were obtained, are explained in Sections IV and V. The main conclusions drawn from this study are mentioned in Section VI.

II. MODEL DESCRIPTION

The simulations are of a resistive, non-turbulent plasma whose initial configuration is tearing mode unstable *i.e.*, has the tearing stability parameter $\Delta' > 0$ [21]. The plasma is perturbed in such a way that a tearing mode grows at a known location. The numerical experiments presented in this section are performed with Viriato [22], a pseudospectral code that solves the non-ideal reduced magnetohydrody-

namic (RMHD) equations [23],

$$\partial_t \psi - \mathbf{B} \cdot \nabla \phi = \eta \nabla_{\perp}^2 \psi - S_{ext}(x, y, t), \quad (1)$$

$$\rho(\partial_t \omega + \mathbf{v} \cdot \nabla \omega) = \mathbf{B} \cdot \nabla j_{\parallel} + \nu \nabla_{\perp}^2 \omega, \quad (2)$$

$$\omega = \nabla_{\perp}^2 \phi, \quad (3)$$

$$j_{\parallel} = \nabla_{\perp}^2 \psi, \quad (4)$$

with the addition of a term, S_{ext} , which will be explained next. In the above equations, ψ is the magnetic flux function, $\mathbf{B} = \hat{e}_z \times \nabla \psi + B_z \hat{e}_z$ is the magnetic field, ϕ is the electrostatic potential, S_{ext} is the term that represents the influence of the control current that is injected, ω is the vorticity, $\mathbf{v} = \hat{e}_z \times \nabla \phi$ is the fluid velocity, and j_{\parallel} is the current density in the direction parallel to the strong magnetic field. Two additional relations are required in order to fully determine these variables: $(\nabla \cdot \mathbf{B}) = 0$ and $(\nabla \cdot \mathbf{v}) = 0$. We assume that both the resistivity η and viscosity ν are constant. All the other variables depend on space (x and y) and time (t). This configuration can be thought of as simulating the poloidal plane of a tokamak, with B_z representing the toroidal magnetic field. The in-plane directions x and y are normalized to a macroscopic length scale a , and time is normalized to the Alfvén time $\tau_A = a/v_A$ where v_A is the Alfvén velocity, defined in the simulations as $v_A = B_z$.

The value chosen for the resistivity is $\eta = 0.01$. This value is much larger than the values typically found in tokamak experiments. This value was chosen to allow the simulations to run in reasonable time using a moderate spatial resolution, while keeping the essential behaviour of this instability. Smaller values of η would require a higher resolution, which would extend the time taken to run a full simulation. The viscosity is $\nu = 0.01$.

These equations are a limit case of the magneto-hydrodynamic (MHD) model which corresponds to a plasma that is immersed in a very strong magnetic field in the z direction. A very clear explanation of the MHD and RMHD models can be found in [24, Sections 2.1 and 2.3].

The simulations are run in a 2D slab geometry with dimensions $L_x \times L_y = 2\pi \times 2.34\pi$ and with periodic boundary conditions in both directions. The strong magnetic field is in the direction perpendicular to the simulation plane, z . The spatial resolution is $N_x \times N_y = 384 \times 384$. The island's X-point is initially located at the center of the box, whose coordinates are $(x, y) = (0, 0)$. The initial configuration is an unstable equilibrium which is perturbed. This equilibrium is given by

$$\psi^0 = \frac{\Psi_0}{\cosh^2(x)}, \quad (5)$$

$$B_y^0 = \nabla_{\perp} \psi^0, \quad (6)$$

$$j_{\parallel}^0 = \nabla_{\perp}^2 \psi^0, \quad (7)$$

$$\omega^0 = 0. \quad (8)$$

The rational surface is located at $x = 0$. The value of Ψ_0 is chosen such that the peak value of B_y^0 is

equal to unity. In addition to this equilibrium we introduce a small perturbation,

$$\psi_1 = \Psi_1 \cos(ky) e^{-x^2}, \quad (9)$$

where $\Psi_1 = \Psi_0 \times 10^{-5}$ and $k = L_x/L_y$. It can be shown that the classical stability parameter [3, 21] is positive for this configuration, $\Delta' > 0$. This perturbation will therefore grow into a magnetic island configuration.

III. NATURAL EVOLUTION OF THE SYSTEM

It is useful to understand how the system evolves when no action is taken upon it, that is, when we are not trying to control the island. This simulation, where the instability grows freely until it reaches saturation, will serve as a reference for all the other numerical experiments. The system is allowed to evolve from the perturbed equilibrium, described by the above equations, through equations (1), (2), (3), and (4). Since we are not using the controller, $S_{ext} = 0$ for all x, y and t .

A quantity that is interesting to analyze is the growth rate of the island. This is usually defined as the growth rate of the logarithm of the perturbed magnetic flux, or of its symmetric $\tilde{A}_{||}$, evaluated at the X-point [see Fig. 4(a)],

$$\gamma(t) = \frac{\partial}{\partial t} \ln \left[\tilde{A}_{||}^X(t) \right]. \quad (10)$$

The time evolution of the growth rate is shown in Fig. 2. It is possible to identify the following main stages: initial transient ($t \lesssim 20$), linear growth ($20 \lesssim t \lesssim 40$), nonlinear regime ($40 \lesssim t \lesssim 100$), and saturation ($t \gtrsim 100$) [25].

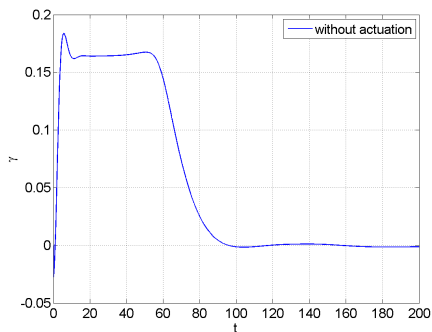


Figure 2: Time evolution of the island's growth rate when the system evolves freely ($S_{ext} = 0$).

Though the plot from Fig. 2 is useful to gain some understanding of the evolution of the island, an alternative way to visualize the behaviour of the instability is to observe the time evolution of the level curves of the total magnetic flux or, similarly, those of $A_{||}$.

In Fig. 3 we can observe these level curves (which also represent the magnetic field line topology) after saturation has been reached ($t \approx 127$). Notice that, although the island is saturating, its width does not yet exceed the width of the box.

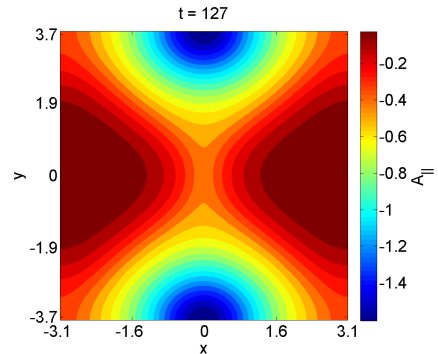


Figure 3: Level curves of the perturbed magnetic flux $\tilde{A}_{||}$ in a simulation where no action is taken upon the island ($S_{ext} = 0$), at the time instant $t = 127$.

In Fig. 4 one can observe the time evolution of the island's width W_{real} . The apparently strange behaviour of the island's width at $t \approx 140$ is due to the island reaching the size of the simulation box. The method for determining W_{real} makes use of the fact that the island separatrix is a surface (or, in the case of this 2D simulation, a level curve) of constant flux.

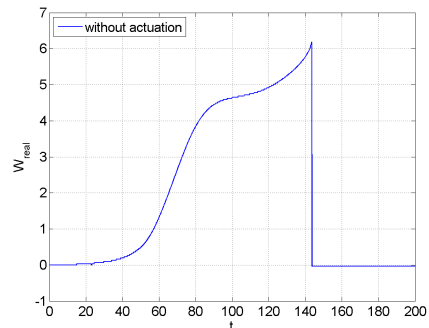


Figure 4: Time evolution of the island's width when the system evolves freely ($S_{ext} = 0$).

Consider the level curves of the magnetic flux for a certain value of t . In the simulation we evaluate the symmetric of the magnetic flux at the island's X-point, which is located at the center of the simulation box. We shall call this value $A_{||}^X$. We then follow the level curve corresponding to this value of $A_{||}$ until we reach the region where the width is largest, the O-point. In our case, it would be either the top or the bottom of the box. Suppose that we choose to use the bottom of the box ($y = -L_y/2$). We search for a value of x , which we will call x_W , such that $A_{||}(x_W, -L_y/2) = A_{||}^X$. We then determine the width of the island as being $W_{real} = 2x_W$.

In Fig. 3, the separatrix of the island does not extend outside the box perimeter, and so the island's

width can be correctly determined. However, when the separatrix goes outside the box's boundaries, there is no x_W such that $A_{\parallel}(x_W, -L_y/2) = A_{\parallel}^X$. The value of W_{real} is set to zero when this happens. In conclusion, W_{real} can be determined as long as the width of the island does not exceed that of the box. In Fig. 4, the moment in which the width suddenly drops to zero is the moment at which W_{real} became larger than L_x . At this point, the simulation is no longer valid because the lateral boundary conditions begin to influence the system.

IV. USING AN ESTIMATE OF THE PERTURBED CURRENT

The most typical way to actively control the island's width is through the injection of current. From a purely dimensional point of view, it is expected that the controller's term in eq. (1) is of the form $S_{ext}(x, y, t) = \eta j_{ext}(x, y, t)$, where η is the plasma resistivity and j_{ext} is the current that is driven into the plasma.

In a real experiment, the driven current will have a narrow and localized profile. A way to represent this narrow profile is to use a Gaussian. The following profile was considered:

$$S_{ext} = s(t) \exp \left[- \left(\frac{x - x_0}{\delta_x} \right)^2 - \left(\frac{y - y_0}{\delta_y} \right)^2 \right]. \quad (11)$$

This profile is that of a Gaussian centered around (x_0, y_0) and with a width of δ_x and δ_y in the horizontal and vertical directions. This Gaussian will can be centered around the island's X-point or at the island's O-point.

For these experiments, we have chosen $x_0 = 0$ and $y_0 = y_X$ or $y_0 = y_O$, where y_X and y_O are the vertical positions of the X-point and O-point, respectively. The values of y_X and y_O are estimated by analysing the plasma's perturbed density (which has a 1:1 correlation with the vorticity, ω) and the perturbed magnetic field. The quantities can be determined using reflectometry and pickup coils, respectively [1, Section 10]. The value which must be used for δ_x is not straightforward to determine. The value which was chosen for the experiments presented in this work is $\delta_x = L_x/\sqrt{10}$. In spite of being an arbitrary value, it corresponds to a deposition width that is much smaller than the macroscopic length, just like the typical deposition profiles of ECCD [18, 19].

We now turn our attention to what the amplitude of the control term should be. Having an amplitude related to the perturbed parallel current is an intuitively sound choice. However, the perturbed current may not be known in real time, *i.e.*, while doing an experiment.

We wish to develop an actuator that relies, as much as possible, on measurable quantities. With this in mind, one should try to use an estimate

of the perturbed current at the X-point, based on quantities that are measurable in real experiments.

Recall that $\tilde{j}_{\parallel} = -\nabla^2 \tilde{A}_{\parallel}$. One can estimate that $\nabla \sim \delta^{-1}$, where δ is the half thickness of the region around the rational surface where the dissipation effects are dominant, which means that

$$\tilde{A}_{\parallel} \sim \tilde{j}_{\parallel} \delta^2. \quad (12)$$

This result, combined with the relation for the theoretical island width [24, Section 4.7],

$$W_{theo} = 4 \sqrt{\frac{-\tilde{A}_{\parallel}}{j_0^x}}. \quad (13)$$

allows one to conclude that

$$\tilde{j}_{\parallel} \sim \frac{j_0^x}{16} \left(\frac{W}{\delta} \right)^2. \quad (14)$$

The value of δ can be estimated through the Sweet-Parker model for reconnection processes [26, 27], which states that $\delta \sim S^{-1/2} L$. In our case, $L \sim a$ [25]. The Lundquist number S is the ratio between the diffusion time $\tau_R = \mu_0 a^2 / \eta$ and the Alfvén time τ_A , and a is the equilibrium length. In short, using the convention that $\mu_0 = 1$, one finds that

$$\delta \sim \sqrt{\frac{a\eta}{v_A}}, \quad (15)$$

and the replacement of this result into (14) gives our final estimate for the amplitude of the actuator term,

$$\eta \tilde{j}_{\parallel} \sim \frac{j_0^x}{16} \frac{W^2}{\tau_A}. \quad (16)$$

Both j_0^x and τ_A are imposed by the equilibrium conditions and hence known. The real width of the island is determined using variables that are available in the simulation but not in a real experiment, namely the reconnection flux \tilde{A}_{\parallel} . The topology of the field lines can be estimated from the peripheral magnetic measurements. However, the magnetic diagnostics might not be entirely reliable on larger devices. It is important to have alternative ways to estimate the island's width. For this study, the island's width was estimated by analysing the density profiles of the plasma at a fixed value of y .

Also, notice that the variable that we actually control in an experiment is the injected current, that is, S_{ext}/η . Since the control term's maximum amplitude, given by the above expression, does not depend on the resistivity, the current that we actually drive into the plasma requires that we know the value of η . Fortunately, the resistivity of the plasma can be estimated from the plasma's temperature T_e and density [28],

$$\eta = \frac{\pi e^2 m^{1/2}}{(4\pi\epsilon_0)^2 (k_B T_e)^{3/2}} \ln \Lambda. \quad (17)$$

In the above equation, ϵ_0 is the vacuum permittivity, m and e are the electron's mass and charge, respectively, k_B is the Boltzmann constant, and Λ is a term that represents the (weak) dependence of the resistivity on the plasma density. For fusion plasmas, $\ln \Lambda \approx 16$.

A. Driving Current into the X-point

Tests have been performed using an injected current with the profile mentioned in eq. (11), and with

$$s(t) = \begin{cases} 0 & \text{if } W(t) < W_{min} \\ -\alpha \frac{j_0^x}{16} \frac{W(t)^2}{\tau_A} & \text{if } W(t) > W_{min} \end{cases}. \quad (18)$$

where α is a numerical factor, $W(t)$ is the estimated width, and W_{min} is a threshold value. This on/off criterion based on the island's estimated width was included because we wish to see the way the island reacts when it is large enough to be detected, and the value chosen for W_{min} allows us to control when we begin to act. Typically, a magnetic island cannot be detected before reaching the non-linear growth stage which means, in our case, before $t \approx 40$ (see Fig. 2). Choosing $W_{min} = 1$ means that the controller is turned on around $t = 67$, when $W_{real} \approx 2.5$ and growth rate is just starting to decrease. The first test was done with $\alpha = 1$, and $j_0^x = 2.6$.

The width of the island was estimated at $y = -1.76$. A comparison between the estimated width W and the real width W_{real} is shown in Fig. 5. It is expected that the estimated width depends on the chosen value of y . In a real fusion device, most diagnostics are positioned at fixed locations, since there is usually a lot of competition for space between various equipment. In these numerical experiments, since the initial position of the island is known, the value of y that is used was chosen so that both the O- and X-points are avoided. This choice is not entirely unrealistic since it is virtually impossible that, in a real experiment, the density diagnostic is aimed exactly at the X- or O-points of the island.

The controller is turned on in very frequent pulses (see Fig. 6). A steady situation in which the controller is turned off and the island's width stays approximately constant is never reached: the island keeps growing back to a point when the on/off threshold is crossed (see Fig. 7). The abrupt changes of the slope of the plot of W_{real} in this experiment suggest that a weaker control current might be more effective in controlling the island.

A reduction of the amount of the injected current was attempted. The results of some of these experiments are shown in Figs. 8 and 9. When using $\alpha = 0.1$ (green lines), the variation of the island's width is much smoother than in the previous case. As we reduce the value of α , the island's width tends to stabilize at larger and larger values,

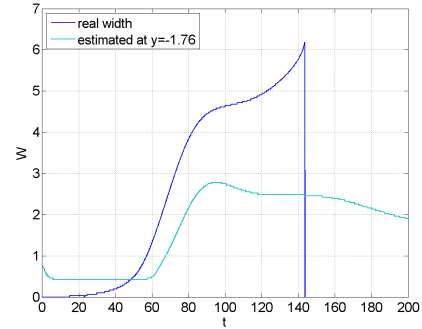


Figure 5: Comparison between the estimated width W and the real island's width W_{real} in an experiment where the system evolves freely ($S_{ext} = 0$).

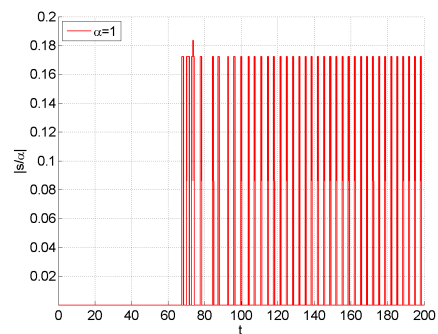


Figure 6: Time evolution of the controller's maximum amplitude, $s(t)$, normalized to α when driving a current into the island's X-point.

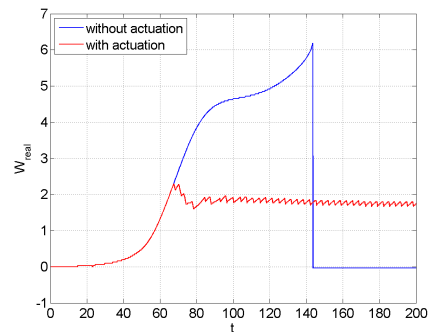


Figure 7: Time evolution of the island's width when driving a current into the island's X-point.

though none of them as large as in the uncontrolled case. The controller was not turned off after initiating operation in any of these experiments. For even smaller values of α , such as 1×10^{-3} , the island is not successfully controlled (not shown in the figure).

Injecting a current into the island's O-point is a control technique whose popularity has increased in the literature [18]. Next, the island's behaviour when current is injected into the O-point is analysed.

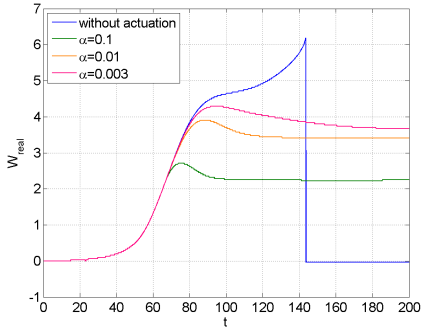


Figure 8: Time evolution of the island's width when driving a current into the island's X-point, using various values for α .

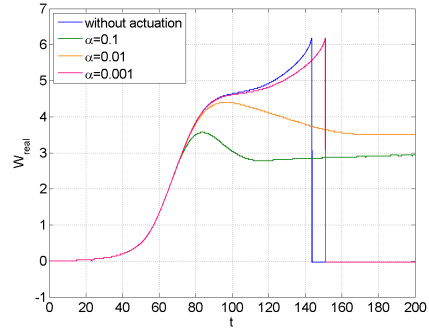


Figure 10: Time evolution of the island's width when driving a current into the island's O-point, using various values for α .

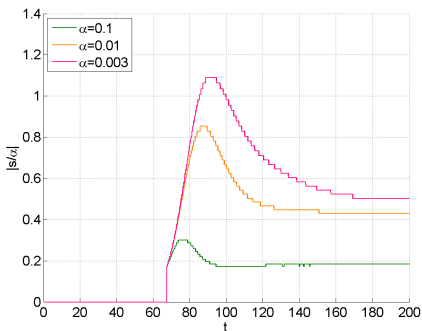


Figure 9: Time evolution of the controller's maximum amplitude, $s(t)$, normalized to α when driving a current into the island's X-point, using various values for α .

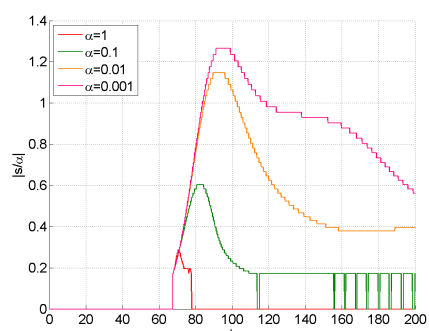


Figure 11: Time evolution of the controller's maximum amplitude, $s(t)$, normalized to α when driving a current into the island's O-point, using various values for α .

B. Driving Current into the O-point

The current that is being injected is spatially Gaussian, recall eq. (11), and its peak value $s(t)$ is defined as

$$s(t) = \begin{cases} 0 & \text{if } W(t) < W_{min} \\ +\alpha \frac{j_0^X}{16} \frac{W(t)^2}{\tau_A} & \text{if } W(t) > W_{min} \end{cases}. \quad (19)$$

Note that $s(t)$ now has a plus sign. It was verified that using a minus sign for the driven current would speed up the island's growth. For these experiments, the following values were used: $j_0^X = 2.6$, $x_0 = 0$, $\delta_x = \delta_y = L_x/\sqrt{10}$, $y_0 = y_O$, where y_O is the estimated vertical position of the O-point, and $W_{lim} = 1$. Four different values of α were tested.

As can be seen in Figs. 10 and 11, using a plus sign, that is, injecting current with the same direction as the perturbed current in the X-point into the O-point, allows one to control the island's width. Using a very small factor, $\alpha = 1 \times 10^{-3}$ (pink lines), the system's evolution is barely different from the uncontrolled one (blue lines). If we increase the amplitude's numerical factor by one (orange lines) or two (green lines) orders of magnitude, the controlling effect of the injected current becomes evident.

With these values of α , the controller is never turned off after being initially turned on, as hap-

pened when current was injected in the X-point. For larger values of α the island suffers a significant vertical shift. For these experiments the plot of W_{real} , which assumes that the X- and O-points remain fixed, is not reliable and thus not shown here.

V. USING OPTIMAL LINEAR CONTROL THEORY

The equations that describe the evolution of the system, equations (1), (2), (3), and (4), are complex, due to a variety of reasons. First of all, the equations are nonlinear. Additionally, the variables involved in these equations are scalar fields which evolve in time, *i.e.*, they are quantities which depend on two spatial directions, x and y . Also, notice that the temporal evolution of the variable which we actually want to control, the island's width, is not explicitly represented in these equations.

Instead of tackling directly such a complex set of equations, it would be preferable to describe the system by a simpler model. An example of such a model would be the following:

$$\partial_t W(t) = G(t)W(t) + c(t). \quad (20)$$

In the above equation, G is the growth rate of the width, which is expected to evolve in time. The controller's input is represented by $c(t)$. In the following paragraphs, we will present the reasoning that led to choosing this model. The steps are not completely formal, but they provide a reasonable explanation as to why the model in equation (20) is an acceptable choice for describing the system.

Consider the equation which describes the time evolution of the magnetic flux, eq. (1):

$$\partial_t \psi - \mathbf{B} \cdot \nabla \phi = \eta \nabla_{\perp}^2 \psi - S_{ext}(x, y, t). \quad (21)$$

It is necessary to evaluate the above equation at the X-point of the island. The second term on the left-hand side of equation (21) is zero at the X-point. Also, if the driven current is a Gaussian centered on the X-point, with maximum amplitude $s(t)$, the second term on the right hand side is equal to $-s(t)$. Equation (21) can therefore be rewritten as

$$\partial_t \psi^X = \eta \nabla_{\perp}^2 \psi^X - s(t), \quad (22)$$

where ψ^X represents the magnetic flux at the X-point. The flux will be a sum of an equilibrium part with a perturbation, the latter assumed to be of the form $\Psi_1 \cos(ky)$, with Ψ_1 being the amplitude of the perturbation. The perturbation has this exact form during the linear regime. When evaluated at the X-point, this perturbation is equal to $-\Psi_1$. We assume that, since the island is growing, this value can vary in time. The equilibrium component, however, is constant in time, so that equation (22) is equivalent to

$$\partial_t \Psi_1 = -\eta \nabla_{\perp}^2 \Psi_1 + s(t), \quad (23)$$

where the equilibrium term on the right-hand side, $\nabla_{\perp}^2 \psi_0$, is neglected as it is much smaller than $\nabla_{\perp}^2 \Psi_1$.

We wish to explicitly write the growth rate of the perturbation in the absence of the control term, which can be defined as $\gamma_0(t) \equiv -\eta \nabla_{\perp}^2 \Psi_1 / \Psi_1$. This growth rate is equivalent to the instantaneous growth rate that was defined in eq. (10) in Section III. Equation (23) can then be rewritten as

$$\partial_t \Psi_1 = \gamma_0(t) \Psi_1 + s(t), \quad (24)$$

The final step is to use the theoretical relation between the perturbation amplitude and the island width, which states that

$$\Psi_1 = -\frac{j_0^X}{16} W^2. \quad (25)$$

By replacing the above relation in equation (24), one finds that

$$\partial_t W = \frac{\gamma_0(t)}{2} W - \frac{8}{j_0^X W} s(t), \quad (26)$$

which is equivalent to eq. (20) if $G(t) = \gamma_0(t)/2$ and

$$s(t) = -\frac{j_0^X W}{8} c(t). \quad (27)$$

Some remarks must be made regarding the reasoning that was just described. It is assumed that the magnetic flux perturbation is of the form $\Psi_1 \cos(ky)$ which might not be entirely true when current is being driven into the system. It is also not true during the nonlinear regime of the tearing mode. The relation in eq. (25) is an approximation that is valid as long as the island's width is small compared to the equilibrium length scale and to the saturation width. Another important thing to point out is that this model describes the time evolution of a scalar.

We will determine a control law for this model using optimal linear control theory. The most basic linear control techniques allow the stabilization of the so called linear, time invariant systems. The convergence of the variable that needs to be controlled to the desired value can be made arbitrarily fast. What these methods overlook, however, is that a faster convergence requires more effort from the controller. For practical applications, as is the case, the input amplitude must be bounded.

This suggests that one should formulate the control problem as an optimization problem that includes both the convergence of the controlled variable and the amplitude of the input. Consider the quantity J , defined as

$$J = \int_0^{\infty} [r_1 W^2(t) + r_2 c^2(t)] dt, \quad (28)$$

which is composed of two parts. The first term in the integral represents the integrated squared width, and the second term in the integral represents the integrated square input. These terms are weighted through the positive constants r_1 and r_2 , respectively. We wish to find a control law $c(t)$ that minimizes J .

A problem of this form is called a linear optimal regulator problem [29]. It can be shown that the input $c(t)$ which minimizes eq. (28) for the system described by eq. (20) is a linear control law of the form

$$c(t) = -F(t)W(t), \quad (29)$$

$$F(t) = r_2^{-1} P(t), \quad (30)$$

where $P(t)$ is the solution of the Riccati equation,

$$\gamma(t)P(t) - r_2^{-1} P^2(t) + r_1 = 0. \quad (31)$$

By solving equation (31) and combining the solution with eq. (30), one finds that

$$F(t) = \frac{\gamma}{2} + \sqrt{\frac{\gamma^2}{4} + \frac{r_1}{r_2}}. \quad (32)$$

The solution with the minus sign was neglected because it makes $F(t) < 0$, which would result in a control law that further destabilizes the system.

There are two limit cases: "cheap" control ($r_1 \gg r_2$) and "expensive control" ($r_1 \ll r_2$). In the former case, one prioritizes the quality of the control

over the amount of power that is required to achieve it. In the latter case, the optimization is done in order to minimize the input's amplitude. Efforts have been made in order to understand the minimum power requirements for tearing mode control using ECCD [30, 31], and it is desirable to use as little power as possible in order to stabilize these modes. This corresponds to the expensive control case. The solution for this limiting case is approximately given by $F(t) = \gamma(t)$. The control is, therefore

$$c(t) = -\gamma(t)W(t) \quad (33)$$

which corresponds to

$$s(t) = -\frac{j_0^X}{8}\gamma(t)W^2(t). \quad (34)$$

According to eq. (34), the injected current will depend on the island's width, on the equilibrium current, on the growth rate of the island, and on the resistivity, the latter because $j_{eccd} = s/\eta$. We have stated how one can obtain all these quantities previously in this document, with the exception of the growth rate. A way to estimate the growth rate of the island without measuring the magnetic flux is to use measurements of the perturbed magnetic field. The magnetic field components can be measured in the periphery of the plasma using pick-up coils. Some numerical experiments, not presented here due to space limitations, evidence that B_x , the horizontal component of the magnetic field, grows with a rate which is similar to that of ψ .

The opposite limit case is also interesting to analyse. If $r_1 \gg r_2$, then $F(t) \approx \sqrt{r_1/r_2}$. By choosing appropriate values for r_1 and r_2 such that $F(t) = 0.5$, one obtains

$$s(t) = -\frac{j_0^X}{16}W^2(t), \quad (35)$$

which, with the difference of a factor of τ_A^{-1} that appears for dimensional reasons, is the same solution as eq. (16). The solution given by equation (34) is also related to eq. (16) by a factor of $2\gamma(t)\tau_A^{-1}$. It is interesting to observe that, using two very distinct approaches, one obtains similar control laws.

The amplitude of the control current is now fully determined, and one can proceed with the experiments. The current was driven into the island's X-point. The controller is turned on after the estimated width exceeds a specified threshold value for the first time. As threshold value of $W_{lim} = 1$, which correspond to turning the controller on at the time instant $t \approx 67$, was chosen. Several amplitudes for the driven current's maximum amplitude were also tested.

Notice that this on/off criterion is different from the one described in the previous section. Before, the controller was turned on only when the island's estimated width exceeded a certain threshold, and would be turned off whenever the width was below

that threshold value. Now, the controller is turned on when the threshold value is met and is never turned off afterwards. The main reason for this change in the criterion is the fact that the control current's amplitude now depends on the island's growth rate (and vice-versa) and thus, a switchoff criterion becomes superfluous.

If the present criterion were used in the previous experiments, the controller would only turn off when the estimated island's width became zero. The width that is estimated by analysing the density profile is never zero (recall Fig. 5), which implies that the controller would never be turned off. In the control law used in this chapter, however, there is another condition for which the controller turns off, and that is $\gamma(t) = 0$. If this condition is met, the controller turns off on its own, without the need of additional logic. As we shall see next, the controller will never be completely turned off, but the driven current will reach a very small amplitude after some time.

Another important consequence of the dependence of $s(t)$ on $\gamma(t)$ is that the island cannot be suppressed. If the island's width started decreasing, $\gamma(t)$ would become negative. This would cause the driven current to change sign and, therefore, to become destabilizing.

The control term, S_{ext} is a Gaussian centered around the X-point, see eq. (11). The deposited current is centered on the island, both horizontally ($x_0 = 0$) and vertically ($y_0 = y_X$). The deposition width is given by $\delta_x = \delta_y = L_x/\sqrt{10}$. When the controller is turned on, its maximum amplitude is

$$s(t) = -\alpha\frac{j_0^X}{8}\gamma_B(t)W^2(t) \quad (36)$$

where α is a numerical factor, γ_B is the growth rate estimated from the magnetic field measurements, and W is the island's estimated width.

The results for these experiments are shown in Figs. 12 and 13. The island's width is controlled for $\alpha = 0.1$ and $\alpha = 0.5$. For smaller values of α , the control was not strong enough and the island managed to grow to its full size and, for larger values of α , the injected current was so strong that numerical problems appeared shortly after the controller was turned on, causing overflows.

These results show that we have successfully managed to take a highly complex system, described by a complicated set of equations, and successfully stabilize it by applying basic linear control techniques to a simple equation that approximately models the dynamics of the system. The control was successful despite the fact that most quantities involved in the control process are only rough estimates of the actual variables.

One observes that the driven current has a smooth profile over time after being turned on, see Fig. 13. Additionally, the driven current's amplitude diminishes with time and tends to a very small value once the island's width stabilizes. This indi-

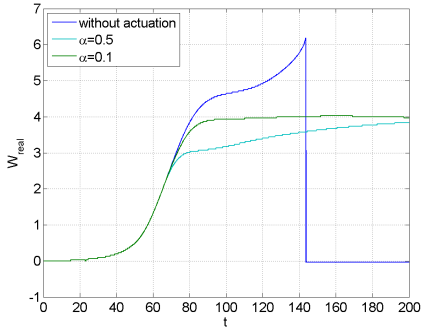


Figure 12: Time evolution of the island’s width when driving a current into the island’s X-point, using various values for α .

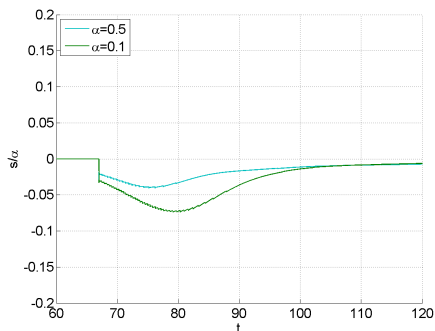


Figure 13: Time evolution of the controller’s maximum amplitude, $s(t)$, normalized to α when driving a current into the island’s X-point, using various values for α .

cates that, if it were possible to have tearing modes during a real fusion reaction provided that they do not exceed a certain size, keeping the instabilities under control requires very little power once their growth has been halted.

Although the reasoning that was presented above was based on the fact that the current is centered around the X-point, experiments were also performed for the case where the current is deposited at the O-point of the island. The results are not presented here for the reason that follows. In terms of the width control, the results are as successful as when current was driven into the X-point. However, unlike the previous experiments, the injected current’s amplitude is anything but smooth: there are very rapid oscillations of $s(t)$ which diminish as time passes. These oscillations are undesirable in practice because they can degrade the devices that

are used to generate the current.

The oscillations appear because the estimated growth rate oscillates. It was verified that the oscillations occur at practically every timestep of the simulation. It is possible that the driven current is constantly changing between being stabilizing and destabilizing. The exact reason why this happens is unknown and will be further investigated in the future.

The results presented in this section open a new range of possibilities for tearing mode control. Using control formalism to deal with such a complex instability appears to be a promising approach. More studies on this matter should be performed in order to explore all the possibilities it has to offer.

VI. CONCLUSIONS

The present work studied the problem of tearing mode control by means of current drive. The study covered two possible spatial profiles for the injected current and variations of its maximum amplitude. Two sets of numerical experiments were performed, each using a different approach for obtaining the control law which determines the control current’s amplitude.

It was observed that, the island’s growth can be halted if the driven current is within a certain range of amplitudes. Within this range, a stronger current causes the system’s variables to oscillate for the duration of the experiment, while a weaker control current allows the system’s variable to smoothly transit into a steady state. It was observed that, unlike what some previous studies suggest, injecting a current into the X-point allows the island to be controlled. Driving a current into the O-point also proved to be a successful way to control the instability. The two methods for determining the amplitude of the current give similar control laws. Both methods are successful in controlling the island’s width.

VII. ACKNOWLEDGMENTS

The numerical simulations that were performed for this work were run in the following supercomputers: HPC-FF (Germany), New Hydra (United Kingdom) and Helios (Japan). We would like to thank the opportunity to use these machines in this study.

-
- [1] J. Wesson, *Tokamaks*. Oxford: Clarendon Press, 3rd ed., 2004.
 [2] ITER Physics Expert Group on Disruptions and Plasma Control and MHD and ITER Physics Basis Editors, “Chapter 3: MHD stability, operational limits and disruptions,” *Nucl. Fusion*, vol. 39,

- no. 12, p. 2251, 1999.
 [3] H. P. Furth, J. Killeen, and M. N. Rosenbluth, “Finite Resistivity Instabilities of a Sheet Pinch,” *Phys. Fluids*, vol. 6, p. 459, 1963.
 [4] P. H. Rutherford, “Nonlinear growth of the tearing mode,” *Phys. Fluids*, vol. 16, no. 11, p. 1903, 1973.

- [5] C. C. Hegna, “The physics of neoclassical magnetohydrodynamic tearing modes,” *Phys. Plasmas*, vol. 5, no. 5, pp. 1767–1774, 1998.
- [6] R. J. La Haye, R. Prater, R. J. Buttery, N. Hayashi, A. Isayama, M. E. Maraschek, L. Urso, and H. Zohm, “Cross-machine benchmarking for ITER of neoclassical tearing mode stabilization by electron cyclotron current drive,” *Nucl. Fusion*, vol. 46, no. 4, p. 451, 2006.
- [7] O. Sauter, R. J. Buttery, R. Felton, T. C. Hender, D. F. Howell, and contributors to the EFDA-JET Workprogramme, “Marginal β -limit for neoclassical tearing modes in JET H-mode discharges,” *Plasma Physics and Controlled Fusion*, vol. 44, no. 9, p. 1999, 2002.
- [8] Z. Chang and J. Callen, “Global energy confinement degradation due to macroscopic phenomena in tokamaks,” *Nucl. Fusion*, vol. 30, no. 2, p. 219, 1990.
- [9] R. J. La Haye, “Neoclassical tearing modes and their control,” *Phys. Plasmas*, vol. 13, no. 5, p. 055501, 2006.
- [10] O. Sauter, E. Westerhof, M. L. Mayoral, B. Alper, P. A. Belo, R. J. Buttery, A. Gondhalekar, T. Hellsten, T. C. Hender, D. F. Howell, T. Johnson, P. Lamalle, M. J. Mantsinen, F. Milani, M. F. F. Nave, F. Nguyen, A. L. Pecquet, S. D. Pinches, S. Podda, and J. Rapp, “Control of neoclassical tearing modes by sawtooth control,” *Phys. Rev. Lett.*, vol. 88, p. 105001, Feb 2002.
- [11] M. Maraschek, G. Gantenbein, T. P. Goodman, S. Günter, D. F. Howell, F. Leuterer, A. Mück, O. Sauter, H. Zohm, Contributors to the EFDA-JET Workprogramme, and the ASDEX Upgrade Team, “Active control of MHD instabilities by ECCD in ASDEX upgrade,” *Nucl. Fusion*, vol. 45, no. 11, p. 1369, 2005.
- [12] A. Isayama, Y. Kamada, T. Ozeki, S. Ide, T. Fujita, T. Oikawa, T. Suzuki, Y. Neyatani, N. Isei, K. Hamamatsu, Y. Ikeda, K. Takahashi, K. Kajiwara, and the JT-60 Team, “Long sustainment of quasi-steady-state high β_p H mode discharges in JT-60U,” *Nucl. Fusion*, vol. 41, no. 6, p. 761, 2001.
- [13] A. Gude, S. Günter, M. Maraschek, H. Zohm, and the ASDEX Upgrade Team, “Temporal evolution of neoclassical tearing modes and its effect on confinement reduction in ASDEX upgrade,” *Nucl. Fusion*, vol. 42, no. 7, p. 833, 2002.
- [14] S. Günter, A. Gude, M. Maraschek, S. Sesnic, H. Zohm, the ASDEX Upgrade Team, and D. F. Howell, “High-confinement regime at high β_N values due to a changed behavior of the neoclassical tearing modes,” *Phys. Rev. Lett.*, vol. 87, p. 275001, Dec 2001.
- [15] D. A. Humphreys, J. R. Ferron, R. J. La Haye, T. C. Luce, C. C. Petty, R. Prater, and A. S. Weller, “Active control for stabilization of neoclassical tearing modes,” *Phys. Plasmas*, vol. 13, no. 5, p. 056113, 2006.
- [16] W. Treutterer, K. Behler, A. Buhler, R. Cole, L. Giannone, A. Kagarmanov, K. Lüddecke, G. Neu, G. Raupp, M. Reich, D. Zasche, and T. Zehetbauer, “Integrated operation of diagnostic and control systems,” *Fusion Eng. Des.*, vol. 86, no. 6–8, pp. 465–470, 2011. Proceedings of the 26th Symposium of Fusion Technology (SOFT-26).
- [17] C. D. Warrick, R. J. Buttery, G. Cunningham, S. J. Fielding, T. C. Hender, B. Lloyd, A. W. Morris, M. R. O’Brien, T. Pinfold, K. Stammers, M. Valovic, M. Walsh, H. R. Wilson, and the COMPASS-D and RF teams, “Complete stabilization of neoclassical tearing modes with lower hybrid current drive on COMPASS-D,” *Phys. Rev. Lett.*, vol. 85, pp. 574–577, Jul 2000.
- [18] M. Maraschek, “Control of neoclassical tearing modes,” *Nucl. Fusion*, vol. 52, no. 7, p. 074007, 2012.
- [19] N. J. Fisch, “Theory of current drive in plasmas,” *Rev. Mod. Phys.*, vol. 59, pp. 175–234, Jan. 1987.
- [20] M. Shimada, D. Campbell, V. Mukhovatov, M. Fujiwara, N. Kirneva, K. Lackner, M. Nagami, V.D.Pustovitov, N. Uckan, J. Wesley, N. Asakura, A. Costley, A. Donné, E. Doyle, A. Fasoli, C. Gormezano, Y. Gribov, O. Gruber, T. Hender, W. Houlberg, S. Ide, Y. Kamada, A. Leonard, B. Lipschultz, A. Loarte, K. Miyamoto, V. Mukhovatov, T. Osborne, A. Polevoi, and A. C. C. Sips, “Chapter 1: Overview and summary,” *Nucl. Fusion*, vol. 47, no. 6, p. S1, 2007.
- [21] H. P. Furth, J. Killeen, and M. N. Rosenbluth, “Finite-resistivity instabilities of a sheet pinch,” *Phys. Fluids*, vol. 6, no. 4, pp. 459–484, 1963.
- [22] “VIRIATO: A Fourier-Hermite spectral code for strongly magnetized plasma dynamics.” <http://web.ist.utl.pt/nuno.f.loureiro/Site/VIRIATO.html>.
- [23] H. R. Strauss, “Nonlinear, three-dimensional magnetohydrodynamics of noncircular tokamaks,” *Phys. Fluids*, vol. 19, pp. 134–140, Jan. 1976.
- [24] D. Biskamp, *Nonlinear Magnetohydrodynamics*. Cambridge: Cambridge University Press, 1st ed., 1997.
- [25] N. F. Loureiro, S. C. Cowley, W. D. Dorland, M. G. Haines, and A. A. Schekochihin, “X-point collapse and saturation in the nonlinear tearing mode reconnection,” *Phys. Rev. Lett.*, vol. 95, p. 235003, Nov 2005.
- [26] P. A. Sweet, “The production of high energy particles in solar flares,” *Nuovo Cimento Suppl.*, vol. 8, p. 188, 1958.
- [27] E. N. Parker, “The solar flare phenomenon and the theory of reconnection and annihilation of magnetic fields,” *Astrophys. J. Suppl. Ser.*, vol. 8, p. 177, 1963.
- [28] L. Spitzer, *Physics of Fully Ionized Plasmas*. New York: Interscience, 1st ed., 1956.
- [29] H. Kwakernaak and R. Sivan, *Linear Optimal Control Systems*. New York: Wiley-Interscience, 1st ed., 1972.
- [30] O. Sauter, M. A. Henderson, G. Ramponi, H. Zohm, and C. Zucca, “On the requirements to control neoclassical tearing modes in burning plasmas,” *Plasma Phys. Control. Fusion*, vol. 52, no. 2, p. 025002, 2010.
- [31] N. Bertelli, D. De Lazzari, and E. Westerhof, “Requirements on localized current drive for the suppression of neoclassical tearing modes,” *Nucl. Fusion*, vol. 51, no. 10, p. 103007, 2011.